https://doi.org/10.30799/jacs.272.25110103 J. Adv. Chem. Sci. – Volume 11 Issue 1 (2025) 832–837

Share Your Innovations through JACS Directory

Journal of Advanced Chemical Sciences

Visit Journal at https://www.jacsdirectory.com/jacs

ISSN: 2394-5311

# Spectro-Thermal Characterization, DFT Calculations and Antimicrobial Activities of Oxime Ligand and Its Mn(II) & Co(II) Metal Complexes

Reema Chand[1,*], Mohseen Ahmed[1], Bibhesh K. Singh[2]

[1]*Department of Chemistry, M.B Govt P.G College, Haldwani, Nainital – 263 139, Uttarakhand, India.*
[2]*Department of Chemistry, Govt Degree College, Nandasain, Chamoli – 246 487, Uttrakhand, India.*

ARTICLEDETAILS

*Article history:*
Received 20 February 2025
Accepted 03 March 2025
Available online 16 March 2025

*Keywords:*
Oxime Ligand
Transition Metal Complexes
DFT Calculation
Antimicrobial Studies

ABSTRACT

An appropriate conventional method was employed to synthesize a new oxime-based ligand, 2,4-dihydroxybenzaldehyde oxime, and its transition metal (II) complexes with Mn and Co ions. The coordination behavior, bonding nature, and crystal structures of these complexes were elucidated using spectroscopic techniques, including FT-IR, UV-Visible, and powder X-ray diffraction. UV-Visible spectral analysis suggests that both metal complexes exhibit an octahedral geometry. Additionally, molecular modeling through Density Functional Theory (DFT) calculations provided detailed insights into their electronic properties, stability trends, and potential reactivity. The optimized structural parameters, including bond lengths and bond angles, were determined using DFT calculations with the B3LYP functional and 6-31G**, 6-311G**(d,p), and LanL2DZ basis sets.

## 1. Introduction

Oxime ligands, derived from the condensation of carbonyl compounds with hydroxylamine, represent a critical class of compounds in coordination chemistry due to their versatile chemical properties and reactivity [1]. These ligands have the unique ability to form stable chelate complexes with metal ions, utilizing the nitrogen and oxygen atoms of the oxime functional group (-C=N-OH) as coordination sites [2]. This characteristic makes oxime ligands particularly valuable in various applications, especially in catalysis, materials science, and biomedicine [3]. The significance of metal-oxime complexes lies in their potential to address several pressing challenges in modern science, In the biomedical domain, these complexes have shown considerable promise as therapeutic agents, particularly in developing new antimicrobial drugs [4]. Their ability to interact with biological molecules opens avenues for targeted drug delivery, diagnostic imaging, and modulation of biological processes, with reported activities including anticancer, antimicrobial, and antioxidant effects [5]. Despite these promising applications, there are notable gaps and limitations in the current research landscape [6]. Existing studies on metal-oxime complexes have predominantly focused on their synthesis and basic coordination chemistry, often with limited exploration of their biological activities [7]. While some research has highlighted the potential of these complexes in antimicrobial and anticancer therapies, a comprehensive understanding of the structure-activity relationships and the mechanisms underlying these activities remains underdeveloped [8]. Moreover, the majority of studies have been confined to specific metals, leaving the potential of other transition metals [9]. particularly those with known biological significance like manganese, cobalt, nickel, and zinc, less explored [10]. There is also a need for more systematic investigations into the interactions of these complexes with microbial systems, particularly concerning their mechanisms of action and the potential to overcome microbial resistance [11]. The existing literature often lacks in-depth evaluations of how these complexes interact with microbial membranes, enzymes, and metabolic pathways, which are critical for developing effective antimicrobial agents [12]. Additionally, while some studies have reported promising results, the reproducibility and scalability of these findings in clinical settings remain questionable [13]. This study aims to address these gaps by synthesizing new oxime-based metal complexes through the reaction of 2,4-dihydroxybenzaldehyde oxime [14]. With transition metals such as manganese (Mn), cobalt (Co), These metals are known for their diverse biological activities, Mn complexes exhibit catalytic and antioxidant properties [15]. (Co) complexes are effective in oxidation reactions and antimicrobial applications, by investigating the structures and properties of these newly synthesized complexes using elemental analysis, spectroscopic techniques, thermal studies, powder XRD, and DFT studies [16]. This research seeks to expand our understanding of metal-oxime coordination chemistry [17]. its implications for developing next-generation antimicrobial agents, Furthermore, this study critically evaluates the antimicrobial activity of these complexes, exploring their potential to enhance the efficacy of existing treatments and overcome resistance mechanisms [18]. By addressing the current limitations in the field and providing a more detailed understanding of the interactions between metal-oxime complexes [19]. biological systems, this research contributes both to the fundamental knowledge of coordination chemistry and the urgent need for new antimicrobial agents in the face of rising microbial resistance [20].

## 2. Experimental Methods

The chemicals 4-hydroxy salicylaldehyde (98%), hydroxylamine hydrochloride (98%), hydrochloric acid (98%), and all metal acetate solid, i.e., $Mn(CH_3COO)_2{\cdot}2H_2O$ (98%) and $Co(CH_3COO)_2{\cdot}2H_2O$ (98%), were procured from Sigma Aldrich. Solvents used for synthesis and spectroscopic analysis have been used after drying with standard procedures.

### *2.1 Synthesis of Oxime Ligand and Its Metal Complexes*

#### *2.1.1 Preparation of Ligand*

Hydroxylamine hydrochloride (0.0696 mg) was dissolved in 20 mL of distilled water in a round-bottom flask, followed by stirring for 2 minutes. A small amount of sodium carbonate was then added to the solution, and the resulting mixture was gently heated to (30-50 °C) using a water bath to facilitate the evolution of carbon dioxide gas and removal of water vapor. After cooling to room temperature, 4-hydroxy salicylaldehyde (0.137 mg) was added dropwise to the reaction mixture while stirring with a glass rod. The appearance of a white precipitate within 5 minutes indicated the completion of the reaction (Scheme 1). The ligand is white with a decomposition temperature of 280 °C and an 85% yield.

*Corresponding Author:reemachand292@gmail.com(Reema Chand)

https://doi.org/10.30799/jacs.272.25110103


*Cite this Article as:* Reema Chand, Mohseen Ahmed, Bibhesh K. Singh, Spectro-thermal characterization, DFT calculations and antimicrobial activities of oxime ligand and its Mn(II) & Co(II) metal complexes, J. Adv. Chem. Sci. 11(1) (2025) 832–837.

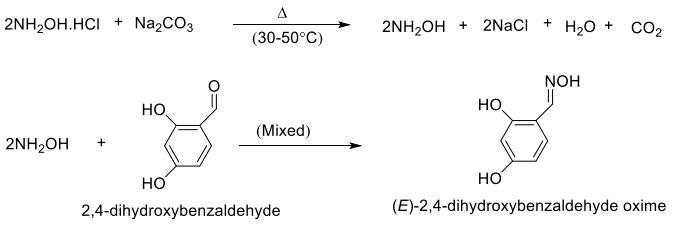


**Scheme 1** Synthesis of the ligand

### *2.1.2 Preparation of Metal Complexes*

The complexes were prepared by dissolving metal acetate dihydrate in a solution composed of 10 mL ethanol and 10 mL double-distilled water. Subsequently, a consistent amount of the ligand was added to the metal acetate solution across all reaction runs. The reaction mixture was then heated in a water bath at 80 °C for 5 hours. Following this, 3 mL of triethylamine or ammonia were added, leading to the formation of a precipitate, indicating successful complexation. The resulting solid complexes were filtered off while heated, washed several times with hot ethanol, and finally dried over $P_4O_{10}$. (Scheme 2), Complex I is gray, decomposes at 140 °C with 80% yield.

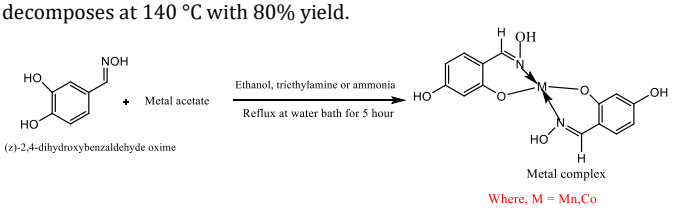


**Scheme 2** General synthesis of the metal complexes of Mn and Co

## 3. Results and Discussion

Based on elemental analysis data, the complexes have the general composition $ML_2$, where M=Mn(II), Co(II), Ligand = 2,4-dihydroxybenzaldehyde oxime. The complexes were obtained in powder form. These were found to be sufficiently soluble in ethanol and DMSO for spectral measurements. The powder XRD helps to obtain cell parameters of the complexes. However, the analytical and spectroscopic data enable us to predict the possible geometry of the complexes. The DFT computation supports the potential complex geometry and aids in determining bond lengths and angles.

### *3.1 FT-IR Spectra*

The FT-IR spectra (Fig. 1) of ligand (L) and its Mn(II) and Co(II) complexes provide significant insights into the metal-binding behavior of the ligand [21].

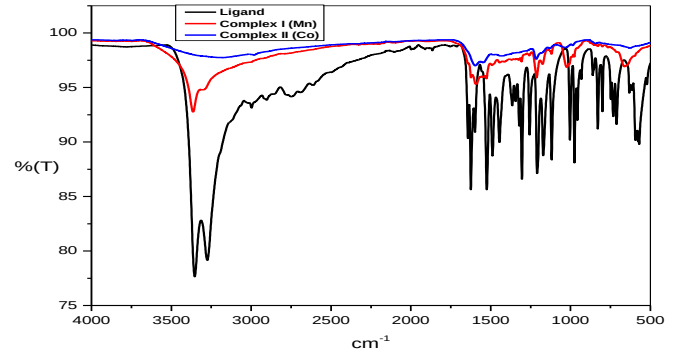


**Fig. 1** FT-IR spectrum of the ligand and metal complexes

The characteristic O–H stretching vibration of the oxime group appears at 3280 $cm^{-1}$ in the ligand, and the broad O-H stretching band at 3114 $cm^{-1}$ in the ligand moves to 3087 $cm^{-1}$ in Complex (I) and 3075 $cm^{-1}$ in Complex (II). A downward shift shows oxime oxygen coordination with metal ions. The azomethine (C=N) stretching vibration at 1660 $cm^{-1}$ in the ligand spectrum shifts to 1637 $cm^{-1}$ in Complex (I) and 1640 $cm^{-1}$ in Complex (II) indicating Coordination with metal centers. Furthermore, the ligand shows an N-O stretching band at 860 $cm^{-1}$, which shifts to 873 $cm^{-1}$ in Complex (I) and 879 $cm^{-1}$ in Complex (II), indicating oxime group involvement in complexation. New FT-IR low-frequency absorption bands show complex building, notably metal-ligand bonding [22]. The bands at 388–332 $cm^{-1}$, 276–293 $cm^{-1}$, 192–179 $cm^{-1}$, and 215–239 $cm^{-1}$ represent (M–O), ν(M–N), ν(O–M–O), and ν(O–M–N).

### *3.2 UV-Vis Spectra*

The UV-Vis spectrum of 2,4-dihydroxybenzaldehyde shows absorption peaks at 275 nm, 301 nm, and 309 nm. The peak at 275 nm corresponds to a π-π* transition in the benzaldehyde system, while the peaks at 301 nm and 309 nm are attributed to n-π* transitions associated with lone pairs on oxygen and hydroxyl groups. These transitions arise from the conjugated system present in the ligand and indicate the electronic excitations within the π-system. The Mn(II) complex exhibits absorption bands at 294 nm, 311 nm, and 372 nm. The peaks at 294 nm and 311 nm correspond to π-π* and n-π* transitions, which are slightly shifted due to metal coordination. The broad absorption band at 372 nm suggests weak d-d transitions, which are characteristic of high-spin Mn(II) complexes in an octahedral coordination environment. The observed transitions correspond to spin-allowed transitions in an octahedral Mn(II) complex, such as $^6A_{1g} \rightarrow {}^4E_g, {}^4T_{2g}$. The UV-Vis spectrum of the Co(II) complex exhibits peaks at 299 nm, 309 nm, and 369 nm. The peaks at 299 nm and 309 nm correspond to π-π* and n-π* transitions, showing slight red shifts due to metal coordination. The absorption band at 369 nm corresponds to d-d transitions, which are characteristic of an octahedral Co(II) complex. Co(II) in an octahedral geometry typically exhibits d-d transitions such as $^4T_{1g}$ (F) → $^4T_{2g}$ (F) (~369 nm, spin-allowed transition) and $^4T_{1g}$ (F) → $^4A_{2g}$ (F) [23]

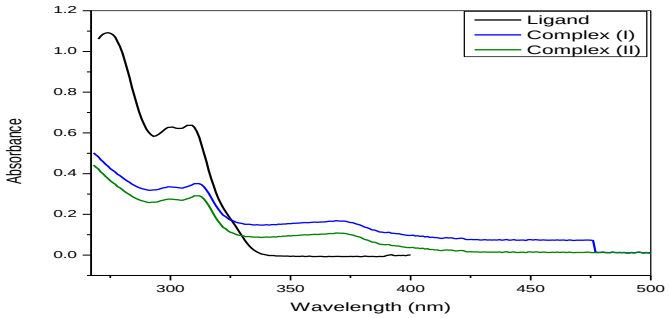


**Fig. 2** UV-visisble spectrum of ligand and its metal complexes

### *3.3 Mass Spectrometrum*

The mass spectra of the oxime ligand and its metal complexes (I-II) depicted in Fig. 3, confirm that the empirical formula aligns with the molecular ion peaks [24]. The molecular ion peak of the ligand appeared at m/z = 153.0562 amu and was assigned to the empirical formula $[C_7H_7NO_3]$. The ion peaks diminished to many stable peaks at m/z = 119.3267, 102.3467, and 77.2751 amu. In the metal complexes (Figs. 3a & 3b), the first fragmentation pattern is analogous, allowing for the deduction of $[M(L)X]^+$. The mass spectra of the complexes exhibit molecular ion peaks at m/z 347.2341 for complex (I) and m/z 349.1945 for complex (II). The significant peaks at m/z 183 and m/z 265 in both complexes result from the demetallation of the complexes [25].

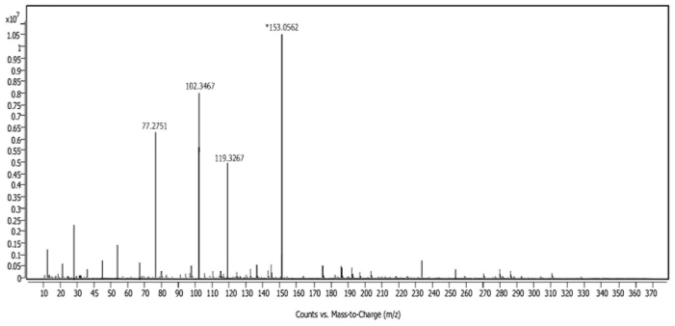


**Fig. 3** Mass spectrum of ligand

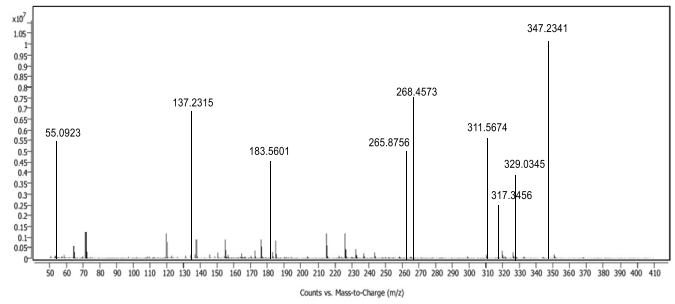


**Fig. 3a** Mass spectrum of Mn metal complex

https://doi.org/10.30799/jacs.272.25110103

*Cite this Article as:* Reema Chand, Mohseen Ahmed, Bibhesh K. Singh, Spectro-thermal characterization, DFT calculations and antimicrobial activities of oxime ligand and its Mn(II) & Co(II) metal complexes, J. Adv. Chem. Sci. 11(1) (2025) 832–837.

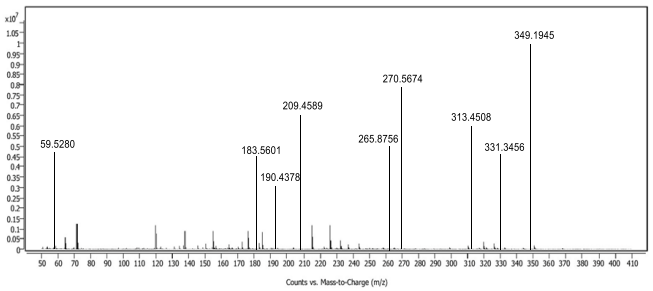


**Fig. 3b** Mass spectrum of Co metal complex

### *3.4 PXRD Analysis*

They used an X-ray diffractometer to look at the ligand and its complexes (I–II) and record the X-ray diffraction angle 2, (range 5–80°) [26]. The XRD pattern of the ligand and its metal complexes (I-II) shows many diffraction peaks, which indicate the crystalline phase [27]. The diffraction peaks correspond to the orthorhombic crystal system of the ligand, the cubic crystal system for complexes (I), and the hexagonal crystal system complex (II) has been obtained. The tentative lattice parameters (a, b, c, α, β, and γ), interplanar spacing (d), Miller indices (h, k, l), and average crystalline size for the ligand and its complexes (I-II) are determined by using the trial-and-error method for finding the best fit between observed and calculated values with the help of X'Pert HighScore's Plus software and listed in (Table 1). Each complex has specific (D) values, which can be used in its characterization. The Debye-Scherrer equation, which reads D = 0.9λ/βcosθ, was used to determine the average crystallite size (D) for both complexes and ligands. The formula takes into account the Bragg diffraction angle (θ) and the full width at half maximum (FWHM) of the diffraction peak (β). And the wavelength of X-rays (1.5406 Å for Cu Kα). The average crystallite size for the oxime ligand was determined to be 41.34 nm, while the metal complexes (I) and (II) were found to be 223.04 nm and 91.05 nm.

**Table 1** Powder-XRD sepctral data of ligand and metal complexes

| Empirical formula | Ligand [$C_7H_7NO_3$] | Complex(I) [$Mn(C_{14}H_{12}N_2O_6)$] | Complex(II) [$Co(C_{14}H_{12}N_2O_6)$] |
|---|---|---|---|
| Formula weight | 154.14 | 359.01 | 363.19 |
| Temp. (K) | 298 | 298 | 298 |
| Wavelength (Å) | 1.54 | 1.54 | 1.54 |
| Crystal system | Orthorhombic | Cubic | Hexagonal |
| Space group | pnmm | Fm3m | P63/mmc |
| Unit cell dimensions | a=14.4180 b=17.4930 c=3.9220 α= β =Y=90 | a=10.7310A b=10.7310 c=10.7310 α=β=Y=90° | a=3.755 b=3.7550 c=6.1190 α=β=90°, Y=120° |
| Volume ($A^3$) | 989.18 | 1235.72 | 740.72 |
| 2θrange | 5-80° | 0-90° | 0-90° |
| Limiting indices | 0<h<2,0<k<1,1<l<5 | 0<h<1,0<k<1,0<l<1 | 0<h<2,0<k<2,1<l<1 |
| Density ($g/cm^3$) | 1.35 | 1.04 | 0.34 |
| Z | 2.00 | 4.00 | 1.00 |
| Particle size (nm) | 41.34 | 28.02 | 26.21 |
| CCDC | 00-039-1667 | 00-032-0639 | 01-085-1244 |

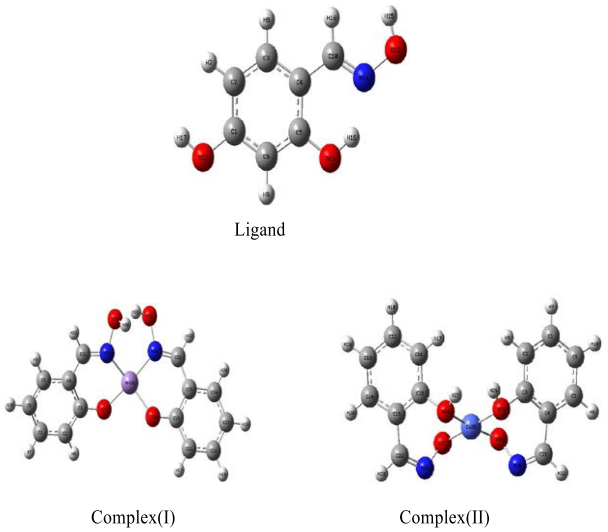


**Fig. 4** Optimized structures of ligand and metal complexes

### *3.5 Molecular Modeling / DFT Calculation*

Transition metal complexes play a crucial role in various chemical processes and catalytic reactions. Understanding their electronic structure and reactivity is essential for predicting their behavior indifferent environments [28]. In this study, we focus on four transition metal complexes (I, II) and employ DFT calculations to gain insights into their electronic properties. All DFT calculations were performed using Gaussian 09 and GaussView 6.0 with the 6-311++G(d,p) basis set for nonmetal atoms and LANL2DZ for metal atoms [29]. Geometry optimizations and optimized structures were conducted to identify the most stable conformations for each complex, along with their corresponding bond angles and bond lengths, with results displayed in shown in Fig. 4. The bond lengths and bond angles of each complex were calculated and are summarized in Tables 2 and 3.

**Table 2** Important optimized bond lengths (Å) & bond Angles (θ̊) of ligand and its complexes

| Ligand and Metalcomplexes | Bond | Bond length (Å) | Angle Position | Bond angle (θ̊) |
|---|---|---|---|---|
| Ligand | $C_1$-$O_{12}$ $C_5$-$O_{11}$ $C_{10}N_{14}$ $N_{14}$-$O_{13}C_1$-$C_2$ | 1.386 1.367 1.300 1.425 1.408 | $C_2$-$C_1$-$C_{12}$ $C_3$-$C_4$-$C_{10}$ C4-C5-O11$C_{10}$-$N_{10}$- $O_{13}C_1$-$C_6$-$C_5$ | 122.201 120.156 121.920 117.980 119.770 |
| Complex I | $O_{21}$-$C_3$ $C_{21}$-$C_4$ $Mn_{29}$-$N_{23}O_{27}$-$Mn_{29}Mn_{29}$-$O_{28}$ $N_{23}$-$O_{25}$ | 1.329 1.423 1.904 1.895 1.882 1.527 | $N_{23}$-$C_{21}$-$C_4$ $Mn_{29}$-$O_{27}$-$C_3$ $N_{24}$-$Mn_{29}$-$O_{28}C_{22}$-$C_{15}$-$C_{16}$ $O_{27}$-$Mn_{29}$-$O_{28}$ | 123.856 131.59 90.340 121.947 98.408 |
| Complex II | $C_{16}$-$O_{24}$ $Co_{25}$-$O_{24}$ $Co_{25}$-$O_{31}O31$-$N_{29}$ $O_{30}$-$N_{29}$ $N_{28}$-$C_{21}$ | 1.441 1.803 1.777 1.304 1.375 1.289 | $C_{25}$-$O_{31}$-$N_{29}$ $C_{16}$-$O_{24}$-$CO_{25}O_{23}$-$C_3$-$C_4$ $O_{30}$-$N_{28}$-$C_{21}$ $C_{16}$-$C_{15}$-$C_{22}$ | 112.46 113.655 121.999 116.011 121.026 |

**Table 3** Ligand and metal complexes optimized energies, charge, spin sate, Dipole moment & Point group

| Ligand and metal complexes | Charge | Spin State | Optimized Energy (Hartree) | Dipole moment (Debye) | Point group |
|---|---|---|---|---|---|
| Ligand | 0 | Single | -551.148 | 6.02 | C1 |
| Complex I | 0 | Doublet | -2252.11 | 7.54 | C1 |
| Complex II | 0 | Doublet | -2483.75 | 7.56 | C1 |

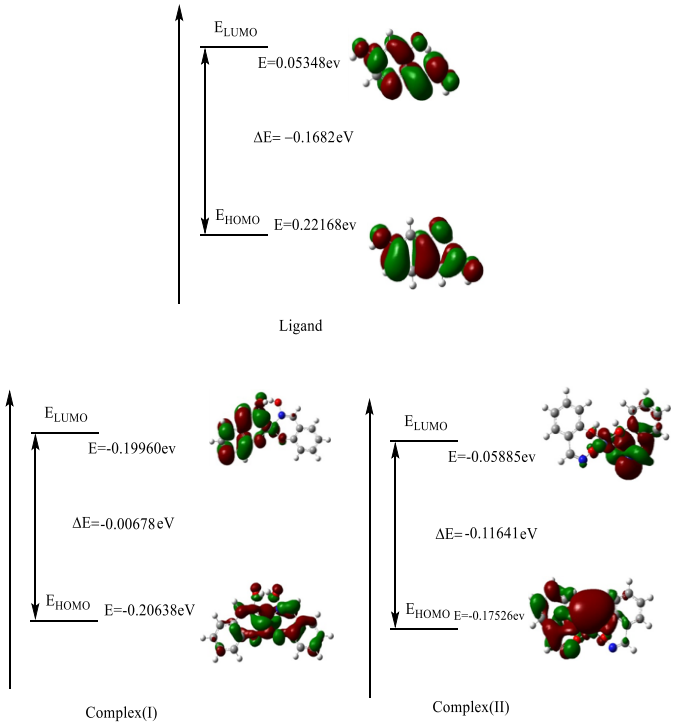


**Fig. 5** Energies of HOMO and LUMO of ligand and metal complexes

https://doi.org/10.30799/jacs.272.25110103

*Cite this Article as:* Reema Chand, Mohseen Ahmed, Bibhesh K. Singh, Spectro-thermal characterization, DFT calculations and antimicrobial activities of oxime ligand and its Mn(II) & Co(II) metal complexes, J. Adv. Chem. Sci. 11(1) (2025) 832–837.

### 3.6 HOMO-LUMO Analysis

The analysis of the HOMO (Highest Occupied Molecular Orbital) and LUMO (Lowest Unoccupied Molecular Orbital) provides further understanding of the electronic structure and reactivity of these complexes [30]. The kinetic stability and chemical reactivity are measured by the energy gap (ΔE) between the HOMO and LUMO levels. For ligand, the HOMO energy is calculated as E = 0.22168 eV, while the LUMO energy is E = 0.05348 eV, resulting in a small energy gap of ΔE = -0.1682 eV, and for complex (I), the HOMO energy is calculated as E = -0.20638 eV, while the LUMO energy is E = -0.19960 eV, resulting in a small energy gap of ΔE = -0.00678 eV. This small gap suggests increased reactivity, possibly indicating a complex that could easily participate in chemical reactions, in (fig. 5). Conversely, Complex (II) shows a gap of ΔE = -0.11641 eV, a HOMO energy of E = -0.17526 eV, and a LUMO energy of E = -0.05885 eV, greater kinetic stability than Complex (I). respectively, summarized in (Table 4), the order of stability is Complex II > Complex I, with complex II being the most stable and complex I the least [31].

**Table 4** Energies of HOMO and LUMO of ligand and metal complexes

| Compounds | HOMO Energy | LUMO Energy | ΔE |
|---|---|---|---|
| Ligand | -0.22168eV | -0.05348eV | -0.1682eV |
| Complex I | -0.20638eV | -0.19960eV | -0.1682eV |
| Complex II | -0.17526eV | -0.05885eV | -0.11641eV |

### 3.7 Molecular Electrostatic Potential (MEP) Analysis

MEP diagrams reveal ligand and metal complex electron density distributions. From extremely negative (red) to highly positive (blue), the potential shows the molecules' nucleophilic and electrophilic sites [32]. The MEP displays electron-rich (negative) regions surrounding the oxygen atoms in the ligand, suggesting nucleophilic assault. Complex (I) has similar electron-rich regions around the oxygen atoms, but the manganese center has more electron-deficient (positive) regions, indicating a larger proclivity for electrophilic interactions at the metal site [33]. The MEP shows electron-rich areas around the oxygen atoms and positive regions around the cobalt core in complex (II), suggesting electrophilic behavior. The MEP values for the ligand and two complexes range from -7.354e-2 to 9.321e-2, reflecting electron density distribution differences between species in Fig. 6.

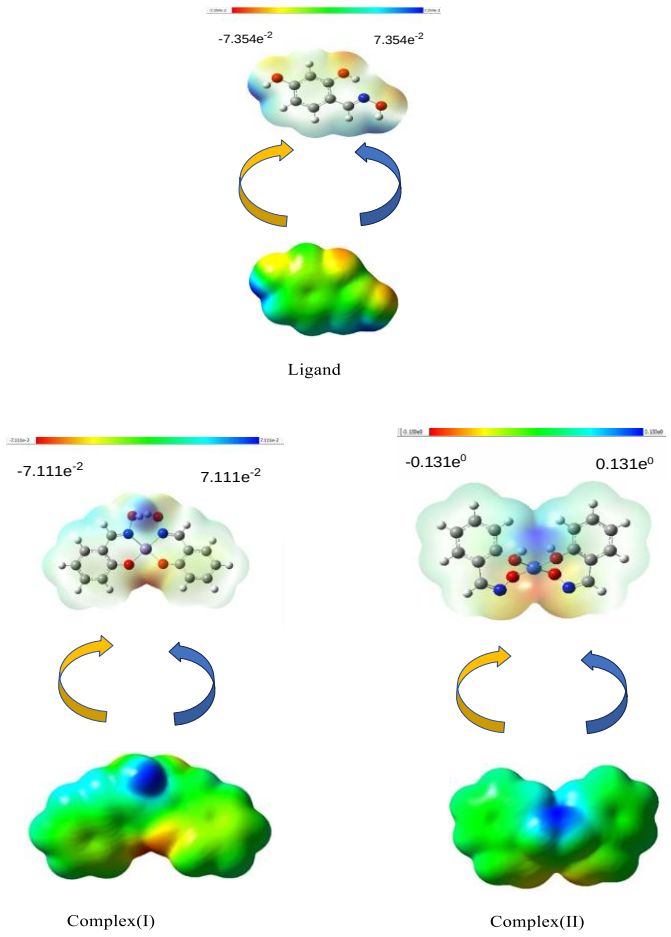


**Fig. 6** Electrostatic potential map ligand and metal complexes

### 3.8 Total SCF Density

Depending on the metal ion, the ligand forms metal complexes with different coordination geometries and electrical characteristics [34]. This emphasizes transition metals' partially filled d-orbitals' importance. The DFT-calculated SCF (Self-Consistent Field) density provides crucial information about metal-ligand interactions, bonding, and electron delocalization in complexes [35].

Contour lines show electron density distribution in the electron density visualization. The free ligand's electron density is concentrated around its functional groups, suggesting metal ion coordination sites. Complexation redistributes electron density, especially around metal centers and ligand coordinating atoms. Changes in metal-ligand bonding and electron sharing result from this redistribution. Each metal complex (I and II) has distinct electron density patterns, revealing coordination geometries and bonding strengths in (Fig. 7). The metal's d-orbitals enhance electron redistribution between metal centers and ligands, highlighting the strength of the metal-ligand connections [36].

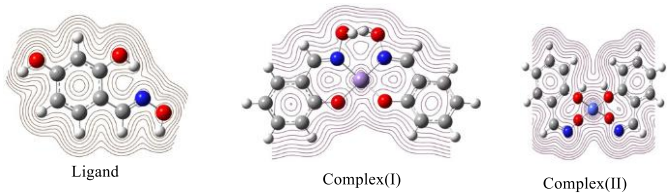


**Fig. 7** Total SCF Density of Ligand and metal Complex

### 3.9 Antimicrobial Activity

In vitro antimicrobial activities were conducted against two human pathogenic microorganisms [37]. One bacterial strain (*E. coli*, MTCC 452) and one fungal strain (*A. niger*, MTCC 281) for the synthesized oxime ligand and its metal complexes.

#### 3.9.1 Minimum Inhibitory Concentration (MIC) Analysis

The study's microorganisms' antibacterial and antifungal activity was tested using the MIC technique at 0.5 McFarland Standard [38]. To the microcentrifuge tube, 100 µL of diluted log cultures of *E. coli* (MTCC-452) and *A. niger* (MTCC-281) were added, along with 5 µL of treatment dilutions (0 to 1000 µg/mL), and incubated for 24 hours [39]. After incubation, all content was transferred to 96-well plates, and turbidity was measured at 630 nm by an ELISA plate reader (iMark Biorad). As positive controls, ciprofloxacin (10 µg) was employed for bacteria and amphotericin B (50 µg) for fungus. According to calculations, the 0.5 McFarland standard culture was diluted 10X for the media (total culture volume = number of tubes (control + treatment) X 0.5 mL). First, the empty Eppendorf tube was weighed, then 500 µL of medium and 20 µL of diluted culture were added. Incubate labeled tubes with 25 µL of treatment dilutions (0-1000 µg/mL) for 2-5 days [40]. After incubation and centrifugation, the pellet-containing tube was weighed after two to five days [41].

#### 3.9.2 Microbial Activity

The complex (I) has the highest antibacterial activity against *E. coli*, with a MIC value of 0.1 µg/mL, followed by the complex (II) with 0.5 µg/mL [42]. Despite being less effective than the complexes, the ligand showed moderate antibacterial activity with a MIC value of 1 µg/mL, surpassing the conventional antibiotic ciprofloxacin (MIC:5µg/mL) [43]. This suggests that metal-ligand interactions, cellular absorption, or bacterial enzyme and biomolecule binding improve the complexes antimicrobial activity over the free ligand in Fig. 8a.. The complex (II) with the lowest MIC value of 0.1 µg/mL showed the strongest antifungal activity against *A. niger*, followed by the complex (I) with 1 µg/mL. The antifungal activity of the ligand was significant, with a MIC value of 10 µg/mL, outperforming the conventional drug Amphotericin B (MIC: 100 µg/mL). These results show that manufactured complexes, especially complex (II), are more effective against fungal strains in Fig. 8b [44].

The stability and activity order of the ligand and its complexes, based on the data, are as follows: Antibacterial activity against *E. coli*: Mn complex (I) > Co complex (II) > Ligand. Antifungal activity against *A. niger*: Co complex (II) > Mn complex (I) > Ligand.

The observed antimicrobial activity can be attributed to the synergistic effects of the ligand's electron-donating groups and the metal ions' coordination properties, enhancing interactions with microbial cell walls and enzymes [45]. The distinct coordination geometries and metal-ligand interactions contribute to the higher stability and activity of the complexes over the free ligand [46].

https://doi.org/10.30799/jacs.272.25110103

*Cite this Article as:* Reema Chand, Mohseen Ahmed, Bibhesh K. Singh, Spectro-thermal characterization, DFT calculations and antimicrobial activities of oxime ligand and its Mn(II) & Co(II) metal complexes, J. Adv. Chem. Sci. 11(1) (2025) 832–837.

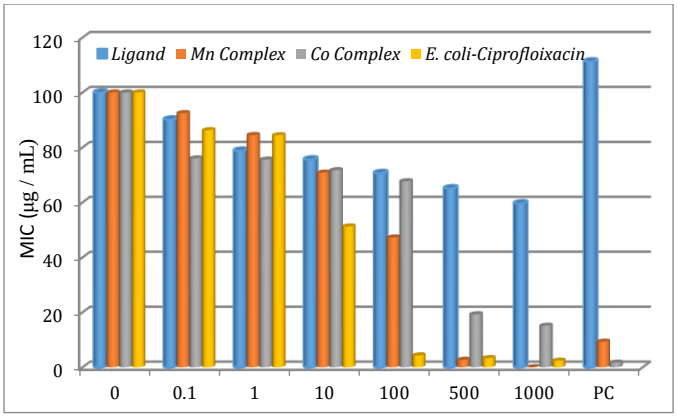


**Fig. 8a** Antibacterial activities (MIC values) of oxime ligand and its complexes

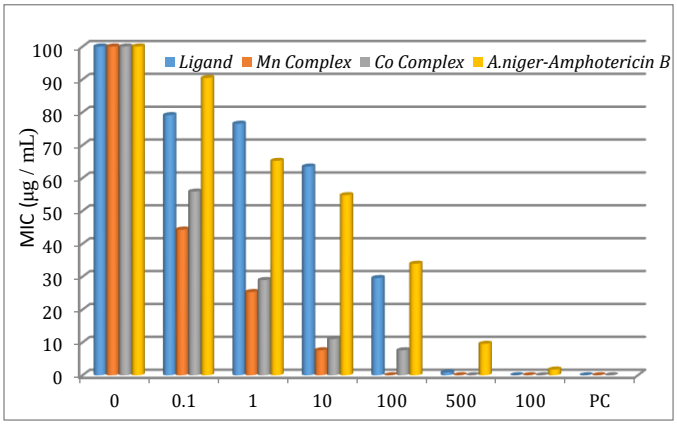


**Fig. 8b** Antifungal activities (MIC values) of oxime ligand and its complexes

## 4. Conclusion

The proposed oxime ligand and its Mn(II) and Co(II) complexes were synthesized and studied using analytical, spectroscopic, and computational approaches. The ligand and its metal complexes had stable, high-spin, octahedral geometries with different structural and electronic characteristics, as shown by FT-IR, UV-Vis, PXRD, and DFT studies. The Co(II) complex has a narrower HOMO-LUMO energy gap than the Mn(II) complex, indicating improved stability. The antimicrobial activity assessment showed that both complexes considerably increased free ligand bioactivity. Mn(II) complex exhibited optimum antibacterial activity against *E. coli* (MIC: 0.1 µg/mL), while Co(II) complex exhibited the strongest antifungal efficacy against *A. niger* (MIC: 0.1 µg/mL). These findings suggest that metal-ligand coordination enhances antibacterial effectiveness by improving cellular absorption and biomolecule interactions. This study shows that oxime-based metal complexes may be promising next-generation antimicrobials. This research addresses crucial gaps in understanding their biological activities and gives vital insights into structure-activity connections and mechanisms of action, opening the door for metal-based treatments to overcome microbial resistance.

## References

[1] L. Pietrobon, Synthesis and reactivity of new transition metal-based catalytic systems in carbonylation reactions, Ph.D Thesis, University of Trieste, Italy.
[2] B. Nath, A. Tarai, A review on oxime functionality: An ordinary functional group with significant impacts in supramolecular chemistry, Chem. Comm. 60(57) (2024) 7266-7287.
[3] C. Mahmoudi, N. Tahraoui Douma, H. Mahmoudi, C.E. Iurciuc, M. Popa, Hydrogels based on proteins cross-linked with carbonyl derivatives of polysaccharides, with biomedical applications, Int. J. Mol. Sci. 25(14) (2024) 7839.
[4] M. Claudel, J.V. Schwarte, K.M. Fromm, New antimicrobial strategies based on metal complexes, Chem. 2(4) (2020) 849-899.
[5] R.P. Rathna, M. Kulandhaivel, Advancements in wound healing: integrating biomolecules, drug delivery carriers, and targeted therapeutics for enhanced tissue repair, Arch. Microbiol. 206 (2024) 199.
[6] X. Zhang, H. Jia, Low impact development planning through a comprehensive optimization framework: Current gaps and future perspectives, Resour. Conserv. Recycl. 190 (2023) 106861.
[7] M. Yan, Fundamental Investigations into the metal-organic framework redox-hopping charge transport-mechanisms and improvement strategies, Ph.D. Thesis, Virginia Polytechnic Institute and State University, Blacksburg, VA, 2024.
[8] A. Dhiman, R. Sharma, R.K. Singh, Target-based anticancer indole derivatives and insight into structure-activity relationship: A mechanistic review update (2018–2021), Act. Pharm. Sin. B 12(7) (2022) 3006-3027.
[9] R. Chand, M. Ahmed, B.K. Singh, A Review: Recent advances in chemistry and applications of 2,4-Dihydroxybenzaldehyde Oxime and its transition metal complexes, J. Adv. Chem. Sci.10(4) (2024) 808-812.
[10] G. Genchi, G. Lauria, A. Catalano, A. Carocci, M.S. Sinicropi, Prevalence of cobalt in the environment and its role in biological processes, Biol. 12 (2023) 1335.
[11] N. Vaou, E. Stavropoulou, C. Voidarou, C. Tsigalou, E. Bezirtzoglou, Towards advances in medicinal plant antimicrobial activity: A review study on challenges and future perspectives, Microbe. 9(10) (2021) 2041.
[12] G. Donadio, F. Mensitieri, V. Santoro, V. Parisi, M.L. Bellone, N. De Tommasi, V. Izzo, F. Dal Piaz, Interactions with microbial proteins driving the antibacterial activity of flavonoids, Pharm. 13(5) (2021) 660.
[13] A. Fedorov, W.J.R. Longabaugh, D. Pot, D.A. Clunie, S.D. Pieper, et al., National cancer institute imaging data commons: Toward transparency, reproducibility, and scalability in imaging artificial intelligence, RadioGraphics 43(12) (2023) e230180.
[14] S.S.R. Albalawi, Strategic surface selection for nanoparticle immobilization to enhance catalytic reactivity, Western Michigan University, USA, 2020.
[15] M.S.S. Adam, M.M. Makhlouf, A. Alharbi, N.M. El-Metwaly, Novel isatin-based complexes of Mn (II) and Cu (II) ions: characterization, homogeneous catalysts for sulfides oxidation, bioactivity screening and theoretical implementations via DFT and pharmacokinetic studies, J. Mol. Liq. 351 (2022) 118620.
[16] S. Kumari, M. Thakur, S. Kumar, Design, spectroscopic analysis, DFT calculations, catalytic evaluation, and comprehensive in silico and in vitro bioactivity studies, including molecular docking, of novel Co(II) complexes of 2-Hydroxy-5,3-(phenylallylidene)aminobenzoic acid, J. Inorg. Organomet. Polym. Mater. 24 (2024) 3351.
[17] H. Yildirim Kalyon, T. Basili, M. Gencten, M. Macit, Y. Sahin, Novel asymmetrical oxime ligand-based coordination compounds in conducting copolymer as a useful electrode for electrochemical supercapacitors, Ionics 31 (2024) 799-824.
[18] Z. Breijyeh, B. Jubeh, R. Karaman, Resistance of gram-negative bacteria to current antibacterial agents and approaches to resolve it, Mol. 25(6) (2020) 1340.
[19] J.K. Pierce, Synthesis and application of air-stable secondary phosphine oxide, oxime, and amine-phosphine palladium (II) complexes in transfer hydrogenation and cross-coupling reactions, Ph.D. Thesis, The University of Alabama, USA, 2022.
[20] L.D. Blackman, T.D. Sutherland, P.J. De Barro, H. Thissen, K.E. Locock, Addressing a future pandemic: how can non-biological complex drugs prepare us for antimicrobial resistance threats?, Mater. Horiz. 9 (2022) 2076–2096.
[21] C. Boulechfar, H. Ferkous, S. Boufas, M. Berredjem, A. Delimi, et al., Synthesis, electrochemical, and quantum chemical studies of some metal complexes: Mn (II), Co (II), and Zn (II) with 2-furaldehyde semicarbazone, J. Mol. Struct. 1271 (2023) 134007.
[22] K.I. Hadjiivanov, D.A. Panayotov, M.Y. Mihaylov, E.Z. Ivanova, K.K. Chakarova, S.M. Andonova, N.L. Drenchev, Power of infrared and Raman spectroscopies to characterize metal-organic frameworks and investigate their interaction with guest molecules, Chem. Rev. 121(3) (2021) 1286-1424.
[23] M.M. Ibrahim, M.A. El-Kemary, S.A. Al-Harbi, H.M. Al-Saidi, S.A. Sallam, A.E.-M.M. Ramadan, Synthesis and structural characterization of pyridine-based Mn (III), Fe (III), and Co (III) complexes as SOD mimics and BSA binding studies, J. Mol. Struct. 1228 (2021) 129706.
[24] A.K. Singh, V.C. Anadebe, M. Singh, N. Arshad, R.C. Barik, et al., Coordination chemistry of chalcones and derivatives and their use as corrosion inhibitors: A comprehensive review, Coord. Chem. Rev. 517 (2024) 215985.
[25] K. Chand, N.J. Meitei, Y.L. Chang, C.L. Tsai, H.Y. Chen, S.C.N. Hsu, Ligand degradation study of unsymmetrical β-Diketiminato copper dioxygen adducts: The length chelating arm effect, ACS Omega 8(23) (2023) 21096–21106.
[26] H.A. Abd El Salam, G.G. Mohamed, E.M. Zayed, Synthesis, spectroscopic characterization, biological application and molecular docking studies of some transition metal complexes of isophthalamide ligand, J. Mol. Struct. 1273 (2023) 134231.
[27] S.A. Aly, S.S. Hassan, H.A. El-Boraey, A. Eldourghamy, E.M. Abdalla, F.M. Alminderej, H.H. Elganzory, Synthesis, biological activity, and the effect of ionization radiation on the spectral, XRD, and TGA analysis of Cu(I), Cu(II), Zn(II), and Cd(II) Complexes, Arab. J. Sci. Eng. 49(1) (2024) 361-379.
[28] A. Nandy, C. Duan, M.G. Taylor, F. Liu, A.H. Steeves, H.J. Kulik, Computational discovery of transition-metal complexes: from high-throughput screening to machine learning, Chem. Rev. 121(16) (2021) 9927-10000.
[29] E.V. Panova, D.A. Safin, Computational studies of copper(II) complexes derived from N-cyclohexyl-3-methoxysalicylideneimine and N-cyclohexyl-3-ethoxysalicylideneimine, Russ. J. Gen. Chem. 94(3) (2024) 703-710.
[30] M.A. Mumit, T.K. Pal, M.A. Alam, M.A.A.A.A. Islam, S. Paul, M.C. Sheikh, DFT studies on vibrational and electronic spectra, HOMO–LUMO, MEP, HOMA, NBO and molecular docking analysis of benzyl-3-N-(2, 4, 5-trimethoxyphenylmethylene) hydrazinecarbodithioate, J. Mol. Struct. 1220 (2020) 128715.
[31] I. Vercellino, L.A. Sazanov, The assembly, regulation and function of the mitochondrial respiratory chain, Nat. Rev. Mol. Cell Biol. 23 (2022) 141-161.
[32] T. Fradi, O. Noureddine, F.B. Taheur, M. Guergueb, et al., New DMAP meso-arylporphyrin Magnesium (II) complex. Spectroscopic, Cyclic voltammetry and X-ray molecular structure characterization. DFT, DOS and MEP calculations and Antioxidant and Antifungal activities, J. Mol. Struct. 1236 (2021) 130299.
[33] A.D. Bagul, M. Kumar, A.M. Alanazi, A. Tufail, N. Tufail, D.D. Gaikwad, A. Dubey, Experimental and computational evaluation of anti-malarial and antioxidant potential of transition metal (II) complexes with tridentate Schiff base derived from pyrrolopyrimidine, BioMetals 37(6) (2024) 1713-1737.

https://doi.org/10.30799/jacs.272.25110103

*Cite this Article as:* Reema Chand, Mohseen Ahmed, Bibhesh K. Singh, Spectro-thermal characterization, DFT calculations and antimicrobial activities of oxime ligand and its Mn(II) & Co(II) metal complexes, J. Adv. Chem. Sci. 11(1) (2025) 832–837.

[34] B. Hosseinzadeh, M. Ahmadi, Coordination geometry in metallo-supramolecular polymer networks, Coord. Chem. Rev. 471 (2022) 214733.
[35] T.Z.H. Gani, Mechanistic studies and design of supported transition metal complexes, Ph.D. thesis, Massachusetts Institute of Technology, USA, 2020.
[36] M. Sarkar, Binuclear transition metal complexes containing metal–metal bonds: Understanding the fundamental aspects and metal–metal cooperativity in catalysis, Inorg. Chim. Acta. Acta 572 (2024) 122275.
[37] N. Ibrahim, A. Kebede, In vitro antibacterial activities of methanol and aqueous leave extracts of selected medicinal plants against human pathogenic bacteria, Saudi J. Biol. Sci. 27(9) (2020) 2261–2268.
[38] T.B. Beressa, S. Deyno, P.E. Alele, Antifungal activity of the essential oil of echinops kebericho mesfin: An in vitro study, Evid. based Complement Alternat. Med. 2020 (2020) 3101324.
[39] C. Singh, D. Adhikari, B.K. Singh, M. Tiwari, Synthesis, characterization, DFT computational studies and biological activity of transition metal complexes derived from 4-(((6-nitrobenzo[d]thiazol-2-yl)imino)methyl)benzene-1,3-diol, J. Coord. Chem. 77 (2024) 2252–2278.
[40] M. Ahmed, R. Chand, B.K. Singh, Synthesis, thermal and spectroscopic analysis, antimicrobial activities and molecular modeling of zinc(II) metal complex of benzoyl glycine, J. Coord. Chem. 77 (2024) 2217–2229.
[41] L.M. MacLean, M. Ariyanayagam, L. Sastry, C. Paterson, M. De Rycker, A.H. Fairlamb, Validation of trypanosoma cruzi inactivation techniques for laboratory use, PLos One 19(4) (2024) e0300021.
[42] M.M. El-Zahed, A.Z. El-Sonbati, F.M.S. Ajadain, M.A. Diab, M.I. Abou-Dobara, Synthesis, spectroscopic characterization, molecular docking and antimicrobial activity of Cu (II), Co (II), Ni (II), Mn (II) and Cd (II) complexes with a tetradentate ONNO donor Schiff base ligand, Inorg. Chem. Commun. 152 (2023) 110710.
[43] R. Shobana, J.H. Thahirunnisa, S. Sivaprakash, A.J. Amali, A.P. Solomon, D. Suresh, Effect of palladium (II) complexes on NorA efflux pump inhibition and resensitization of fluoroquinolone-resistant staphylococcus aureus: in vitro and in silico approach, Front. Cell. Infect. Microbiol. 13 (2024) 1340135.
[44] X.D. Yin, K.Y. Ma, Y.L. Wang, Y. Sun, X.F. Shang, Z.M. Zhao, R.X. Wang, Y.J. Chen, J.K. Zhu, Y.Q. Liu, Design, Synthesis, and antifungal evaluation of 8-hydroxyquinoline metal complexes against phytopathogenic fungi, J. Agric. Food Chem. 68(40) (2020) 11096–11104.
[45] A.M. Fahim, M. Hasanin, I.H.I. Habib, R.O. El-Attar, S. Dacrory, Synthesis, antimicrobial activity, theoretical investigation, and electrochemical studies of cellulosic metal complexes, J. Iran. Chem. Soc. 20 (2023) 1699–1718.
[46] N.P. Juraj, S.I. Kirin, Inorganic stereochemistry: Geometric isomerism in bis-tridentate ligand complexes, Coord. Chem. Rev. 445(9) (2021) 214051.

https://doi.org/10.30799/jacs.272.25110103

*Cite this Article as:* Reema Chand, Mohseen Ahmed, Bibhesh K. Singh, Spectro-thermal characterization, DFT calculations and antimicrobial activities of oxime ligand and its Mn(II) & Co(II) metal complexes, J. Adv. Chem. Sci. 11(1) (2025) 832–837.